

THE LONG-TERM EVOLUTION OF THE GW170817 REMNANT

MENQUAN LIU JIE ZHANG AND CONG WANG

Department of Astronomy, Qilu Normal University, Jinan 250300, China

ABSTRACT

GW170817 represents the first observed binary neutron star merger event by humanity. The observation of GW170817 has identified the correlation between Kilonova, gravitational wave and short GRB. The shocks from GW170817 have the capacity to inject significant thermal and kinetic energies into the interstellar medium and evolve for over a million years. In this letter, we adopt the special relativity fluid dynamics equations to simulate the evolution of the GW170817 remnant over a span of one million years. Our simulations yield the evolution profiles of the velocity, density, mass, radius, luminosity, and energies of the remnant. We estimate that the GW170817 remnant will reach the average maximum luminosity 2.56×10^{39} erg s⁻¹ at approximately 3.96×10^4 yr. At the end of the cooling stage, the contaminated radius and mass are 48.35 pc and $2.25 \times 10^4 M_{\odot}$, respectively.

Subject headings: neutron star merger– shock – remnant– Methods: numerical

1. INTRODUCTION

On August 17, 2017, the LIGO and Virgo collaborations detected gravitational waves from the binary neutron star merger source GW170817 for the first time, and 10.86 hours later, Drout et al. (2017) identified signals in the optical bands, including ultraviolet, optical, and infrared (its transient electromagnetic counterpart is named AT2017gfo). The analysis indicates that the optical curve is largely consistent with the decay of the r-process nucleosynthesis products, and the mass of the ejecta during the merger process is estimated to be $\sim 0.05 M_{\odot}$. Abbott et al. (2017) inferred from the corresponding light curves that the distributions of dynamical ejecta mass vary between $10^{-3} - 10^{-2} M_{\odot}$ for various equations of state. A more recent estimation of ejecta mass range is between $10^{-3} - 10^{-1} M_{\odot}$ (Ristic et al. 2023). The optical and near-infrared observations are effectively explained using the kilonova model. Furthermore, emissions in other bands of electromagnetic signals from GW170817, including X-ray and gamma-ray bands, have also been observed. Thus, the co-occurrence of gravitational waves and electromagnetic signals during the merger of binary neutron stars is unequivocally confirmed. It is hypothesized that the short gamma burst coincides with the binary neutron star merger event. Kasliwal et al. (2017) examined the signals in the gamma band of GW170817/GRB170817a and concluded that GW170817/GRB170817a is not an ordinary short gamma burst with an extreme relativistic jet, but a wide-angled, moderately relativistic, cocoon-like explosion, whose remnant's shape assumes nearly spherical symmetry over long-term evolution. Recent efforts to simulate the generation of optical counterparts from the gamma band to the radio band of GW170817 have been undertaken by two- and three-dimensional models (Ekanger et al. 2023).

Binary neutron star merger events are considered significant sources of the r-process elements. Current research posits that most of the r-process elements with $A > 130$ in the universe may have originated from neutron star mergers, rather than supernova explosions as previously assumed. Compared with neutron star mergers, core-collapse supernovae exhibit a higher explosion rate, but the r-process element yield is comparatively low, and more importantly, they struggle to produce the element distributions for $A > 130$ that align with observations. In addition, neutron star mergers are also tied to cutting-edge research in astronomical and theoretical physics, such as dark energy and general relativity (Creminelli & Vernizzi 2017). GW170817 may have harbored a magnetar at its center before the explosion, and a black hole may have formed at its center after the explosion. However, it was suggested that it was possible that the merger of strange stars rather than neutron stars occurred (Lai et al. 2018).

In summary, GW170817 is a pivotal and typical source, and it is also one of the hot spots in astronomical and theoretical physics research. Although recent observations at 3 GHz band indicated that there is no clear evidence for a late-time re-brightening of the GW170817 nonthermal afterglow emission, the remnant may be observed by multiple bands later (Balasubramanian et al. 2022). Present researches on GW170817 mainly report on observed phenomena and how they are interpreted, and seldom focus on its subsequent evolution of remnant. A study was conducted on the binary neutron star merger whose evolution time is more than 100 years (Rosswog et al. 2014). The long-term evolution of binary neutron star merger remnants for millions of years has been previously explored, but it is not targeted to GW170817 (Liu & Zhang 2017). The difference in the long-term evolution of neutron stars merger and supernova has also been discussed. In this letter, we aim to substitute the observational parameters of

GW170817 into a non-homogeneous special relativistic hydrodynamic equations including electron fraction with r-process elements and the typical interstellar medium properties to simulate the subsequent long-term evolution of the GW170817. Given the long-term evolution, ejecta mass is more important than other quantities such as precise shape, composition, temperature and density of the ejecta. Therefore, we will examine the effect of different ejecta mass on the long-term evolution. This is a novel approach. Our study can predict not only the subsequent evolution of the GW170817, but also the impact on the interstellar medium around it. The evolution laws of luminosity, energies, velocity, etc., of the remnant will be detailed.

2. HYDRODYNAMICAL EQUATIONS AND INITIAL MODEL

Due to the substantial kinetic energy of the ejecta coupled with its minimal mass, the velocity achieved is remarkably high. Specifically, for an ejecta mass of $0.001M_{\odot}$, the average speed reaches approximately $\sim 0.77c$, where c is the velocity of light. Under these conditions, the traditional Newtonian dynamics equations fail to provide an accurate representation, thereby necessitating the adoption of special relativistic hydrodynamic equations.

The special relativistic hydrodynamic equations, incorporating cooling mechanisms for the detailed depiction of shock propagation in remnants, are articulated as follows (Liu & Zhang 2017)

$$\frac{\partial D}{\partial t} + \nabla \cdot (D\mathbf{v}) = 0, \quad (1)$$

$$\frac{\partial \mathbf{S}}{\partial t} + \nabla \cdot (\mathbf{S}\mathbf{v} + P\mathbf{I}) = 0, \quad (2)$$

$$\frac{\partial \tau}{\partial t} + \nabla \cdot (\tau\mathbf{v} + P\mathbf{v}) = -n_e n_H \Lambda(T), \quad (3)$$

$$\mathbf{S} = Dh\Gamma\mathbf{v}, \quad (4)$$

$$\tau = Dh\Gamma - P - D, \quad (5)$$

where Eqs.(1)-(3) represent the conservation of rest mass, momentum, and energy, respectively. The variables D , \mathbf{S} and τ correspond to the lab frame rest mass, momentum, and energy densities (excluding rest mass), respectively. $D = \rho\Gamma$, where ρ is the mass density, $\Gamma = (1 - v^2)^{-1/2}$ is the Lorentz factor. h is the specific enthalpy defined by $h = 1 + \epsilon + P/\rho$, with ϵ being the specific internal energy. P is the pressure. In the above equations, we have used the natural units in which the speed of light c is taken to be unity. For example, $h = 1 + \epsilon/c^2 + P/\rho c^2$ in the normal units. In the equations, t is the time, \mathbf{v} is the velocity and \mathbf{I} is the identity matrix. n_e and n_H are the electron and the hydrogen number densities, respectively. $\Lambda(T)$ is the cooling function. For temperatures above 10^4K , the cooling function is given by Wang et al. (2014). While for temperatures between $10^2 - 10^4\text{K}$, the cooling function by Sarangi & Slavin (2022) is adopted. As the temperatures **drop** below 10^2K , the cooling rate is not effective and **is** treated as zero. Assuming the composition of interstellar medium (ISM) is monatomic and nonrelativistic,

$$P = \rho\mu^{-1}N_A kT, \quad (6)$$

where N_A represents the Avogadro constant, k the Boltzmann constant, and μ the mean molecular weight in units of m_H . In the case of ionized gas, μ is determined by following equation

$$\mu^{-1} = Y_e + Y_N, \quad (7)$$

$$Y_e = X_H + 1/2X_{He} + \sum_i \frac{Z_i}{A_i} X_{Ri}, \quad (8)$$

$$Y_N = X_H + 1/4X_{He} + \sum_i \frac{1}{A_i} X_{Ri}, \quad (9)$$

where Y_e and Y_N are electron fraction and nucleus fraction for each nucleon. X_H and X_{He} are the mass abundance for hydrogen and helium, respectively. Z_i , A_i and X_{Ri} are the nuclear charge number, mass number, and mass abundance of metals (including r-process elements).

The methodology employed to solve the above equations is an explicit Lagrangian finite-difference scheme as we employed before (Liu et al. 2009; Liu & Zhang 2017). The explosive energy of GW170817 is $\sim 1.0 \times 10^{51}$ erg according to Shibata et al. (2017), in which kinetic energy is the vast majority, and thermal energy is negligible. The initial Y_e of ejecta is 0.25, but after decay of r-process elements, it changes to 0.47. The composition of ISM is the recommended elemental abundances in the solar photosphere derived from spectroscopy. The density of ISM is $2.22 \times 10^{-24}\text{g cm}^3$ (corresponding to a number density of hydrogen $n_H = 1\text{cm}^3$). The ISM temperature is set to be 10^3K to make sure it doesn't cool down until the shock arrives. Since the maximal uncertainty comes from ejecta mass and initial velocity, we simulated three different evolution models with ejecta masses as follows: $10^{-3}M_{\odot}$ (noted as Model 1) (Rueda et al. 2022; Ristic et al. 2023), $0.05M_{\odot}$ (noted as Model 2) (Drout et al. 2017) and $10^{-1}M_{\odot}$ (noted as Model 3) (Fryer et al. 2024). $0.05M_{\odot}$ is the most likely ejecta mass of GW170817, while $10^{-3}M_{\odot}$ and $10^{-1}M_{\odot}$ represent the extremes of ejecta masses. Their parameters are shown in the Table 1.

3. RESULTS

The evolution of binary neutron star merger remnants can be divided into three stages, the first of which is the adiabatic expansion stage before the shock wave cools. The second stage is the cooling phase. In this stage, a large amount of energy is emitted, causing the luminosity of the remnant to significantly increase. On the other hand, a relatively dense shell is formed rapidly at the same time. When the total energy released by cooling reaches 90% of the initial energy, we consider the cooling to be over and the evolution enters the third stage, namely, the shell dispersion stage, in which the thickness of the shell increases significantly, and the density becomes smaller and smaller, gradually approaching the ISM density.

The evolution of the three models is similar, so in the following we will focus on the most possible initial model: Model 2. Figure 1 shows the velocity profiles at some characteristic times, ranging from 10^2yr to 10^6yr after the merger, in which $3.55 \times 10^4\text{year}$ is the time when the remnant reaches the maximum luminosity. From the velocity profile of the shock, it is evident that the wave

front of the shock is very steep in the first stage, until the relatively dense shell begins to form. The first shock wave is the most important part of the shock wave propagation process because it contains the main mass and energy of the remnant. We present the variation of the velocity of the first shock wave in the bottom panel of Figure 1. It can be seen that the speed of the first shock wave decreases very quickly, and the speed of the shock wave generally decreases exponentially. However, it does not decrease monotonically; we can see that the speed of the shock wave first decreases and then increases at $\sim 3.6 \times 10^4$ yr, forming a V-shape, attributed to the deceleration of the first shock when the cooling begins, until the secondary shock (sub-shock) catches up with the first shock wave. Shock wave piles up ISM into a shell, and the area behind the shell is called as “bubble”. The change of velocity inside the bubble is complex. In the initial stage, the velocity inside the bubble gradually decreases with time, and then an inward shock wave is formed. The inward shock wave collides with the remnant center and bounces back. The bounce shock moves forward fast and can catch up with the first shock. This shock oscillation occurs several times in the bubble, but the amplitude of the oscillation is getting smaller and smaller with time. After 10^6 yr, the speed is less than 20 km s^{-1} .

Figure 2 shows the density profile of the remnant over a million years. The characteristic times are the same as those in Figure 1. After the adiabatic expansion stage, the maximum luminosity appears when the shell is first formed, because the temperature of the shell at this time is about 10^5 K, at which the value of the cooling function is maximal. The effective cooling converts the heat energy of the remnant into light energy and is released outward. It is evident that during the cooling stage, the shock wave piles up the ISM into a very thin shell, as illustrated by the density profile at 10^5 yr, which is more than 3 orders of magnitude denser than the average density of the ISM. On the contrary, the density in the bubble is very low, similar to a vacuum. There is another shell inside the bubble resulting from the boundary of the ejecta and the initial ISM. At the third stage, the shell slowly disappears and spreads, as shown in the density profile at 10^6 yr. This is the final stage of the remnant evolution.

The mass and radius of the contaminated ISM vs time are shown in Figure 3. Understandably, both quantities exhibit a monotonic increase over time. It can be observed that the variation of the radius and mass of the remnant is relatively smooth. The radius and mass of the remnant at the time of maximum luminosity are 20.69 pc and $1.20 \times 10^3 M_\odot$, respectively. However, the radius and mass of the remnant increase to 44.74 pc and $1.22 \times 10^4 M_\odot$ after the cooling stage. The contaminated ISM mass and radius are significantly influenced by the ejected energy and mass (see Table 1).

Energy and luminosity are complementary concepts, as depicted in Figure 4 and Figure 5. Figure 4 presents

the changes in kinetic energy, thermal energy, and total energy of the remnant at different times. The black, red, and blue lines represent the kinetic, thermal, and total energy of the remnant, respectively. Although the total energy remains essentially constant during the adiabatic expansion stage, resulting in a nearly horizontal trend, the composition of energy undergoes significant transformations, shifting from predominantly kinetic to thermal energy dominance at this stage. During the cooling stage, kinetic energy, thermal energy, and total energy all decline sharply. In the diffusion phase, the overall energy is dissipated gradually. The adiabatic expansion period lasts for 1.2×10^4 years, with the maximum luminosity occurring at 3.55×10^4 years, reaching $1.31 \times 10^{39} \text{ erg s}^{-1}$, and the luminosity remains larger than $10^{38} \text{ erg s}^{-1}$ from 1.86×10^4 yr to 8.13×10^4 yr, spanning about 6.3×10^4 years. Post-peak luminosity, the trend exhibits significant oscillations alongside a general exponential decrease. Compared to supernova remnants, the energy variation trend of the merger remnant’s shock wave closely mirrors that of supernova remnants, with the notable difference being that the onset of cooling for the merger remnant (marked by the peak luminosity) occurs significantly earlier than in supernova remnants. In Figure 5, it is evident that the greater the mass of the ejecta, the higher the luminosity, and the longer the duration before reaching the maximum luminosity.

4. CONCLUSION AND DISCUSSION

From the above analysis, we estimate that the variation range of GW170817 remnant. For example, the time to reach the maximum luminosity is $3.31 \sim 5.01 \times 10^4$ yr. The maximum luminosity is $1.04 \sim 4.08 \times 10^{39} \text{ erg s}^{-1}$. Taking the average, we estimate that the GW170817 remnant will reach the maximum luminosity at approximately $\sim 3.96 \times 10^4$ yr, with the maximum luminosity being around $2.56 \times 10^{39} \text{ erg s}^{-1}$. The remnant radius and mass when the cooling ends are estimated to be 48.35 pc and $2.25 \times 10^4 M_\odot$, respectively.

The metallicity of the surrounding ISM of a binary neutron star may be greater than that of the Sun, thus all the aforementioned quantities will vary with the metallicity. According to the empirical formula (Thornton et al. 1998), the remnant radius R_E is proportional to $(Z/Z_\odot)^{-0.1}$, and the remnant mass M_E is proportional to $(Z/Z_\odot)^{-0.28}$. If the actual metallicity is twice that of the Sun, the remnant radius and mass upon the completion of cooling would be 51.82 pc and $1.85 \times 10^4 M_\odot$, respectively. This principle applies similarly to other quantities.

MQL like to thank professor Y. Z. Qian at the University of Minnesota for his help. This work is supported by the National Natural Science Foundation of China (grant 12373109 and U2031121), National Key Research and Development Program of China (grant SQ2023YFB4500096) and the Natural Science Foundation of Shandong Province (grant ZR2020MA063).

REFERENCES

- Abbott, B. P. et al. 2017, *The Astrophysical Journal Letters*, 850, 39
- Balasubramanian, A. et al. 2022, *The Astrophysical Journal*, 938, 12
- Creminelli, P., & Vernizzi, F. 2017, *Physical Review Letters*, 119

TABLE 1

EVOLUTIONARY PARAMETERS AT DIFFERENT EJECTA MASSES, WHERE M_{ej} IS THE EJECTA MASS, $\bar{v}_{ini}(c)$ IS THE INITIAL AVERAGE VELOCITY. THE SUBSCRIPT m INDICATES THE TIME WHEN THE LUMINOSITY IS MAXIMAL. THE SUBSCRIPT E INDICATES THE END TIME FOR COOLING.

	$M_{ej}(M_{\odot})$	$\bar{v}_{ini}(c)$	$t_m(\text{yr})$	$R_m(\text{pc})$	$L_m(\text{erg s}^{-1})$	$t_E(\text{yr})$	$R_E(\text{pc})$	$M_E(M_{\odot})$
Model 1	1.0×10^{-3}	0.77	3.31×10^4	18.84	1.04×10^{39}	4.79×10^5	41.41	9.71×10^3
Model 2	5.0×10^{-2}	0.32	3.55×10^4	20.69	1.31×10^{39}	4.90×10^5	44.74	1.22×10^4
Model 3	1.0×10^{-1}	0.22	5.01×10^4	31.99	4.08×10^{39}	6.92×10^5	69.30	4.55×10^4

- Drout, M. R. et al. 2017, *Science*, 358, 1570
 Ekanger, N., Bhattacharya, M., & Horiuchi, S. 2023, *Monthly Notices of the Royal Astronomical Society*, 525, 2040
 Fryer, C. L. et al. 2024, *The Astrophysical Journal*, 961, 9
 Kasliwal, M. M. et al. 2017, *Science*, 358, 1559
 Lai, X.-Y., Yu, Y.-W., Zhou, E.-P., Li, Y.-Y., & Xu, R.-X. 2018, *Research in Astronomy and Astrophysics*, 18, 24
 Liu, M.-Q., Yuan, Y.-F., & Zhang, J. 2009, *Monthly Notices of the Royal Astronomical Society*, 400, 815
 Liu, M.-Q., & Zhang, J. 2017, *Monthly Notices of the Royal Astronomical Society*, 472, 708
 Ristic, M. et al. 2023, *The Astrophysical Journal*, 956, 64
 Rosswog, S., Korobkin, O., Arcones, A., Thielemann, F. K., & Piran, T. 2014, *Monthly Notices of the Royal Astronomical Society*, 439, 744
 Rueda, J. A., Ruffini, R., Li, L., Moradi, R., Sahakyan, N., & Wang, Y. 2022, *International Journal of Modern Physics D*, 31, 2230013
 Sarangi, A., & Slavin, J. D. 2022, *The Astrophysical Journal*, 933, 89
 Shibata, M., Fujibayashi, S., Hotokezaka, K., Kiuchi, K., Kyutoku, K., Sekiguchi, Y., & Tanaka, M. 2017, *Physical Review D*, 96, 123012
 Thornton, K., Gaudlitz, M., Janka, H.-T., & Steinmetz, M. 1998, *The Astrophysical Journal*, 500, 95
 Wang, Y., Ferland, G. J., Lykins, M. L., Porter, R. L., van Hoof, P. A. M., & Williams, R. J. R. 2014, *Monthly Notices of the Royal Astronomical Society*, 440, 3100

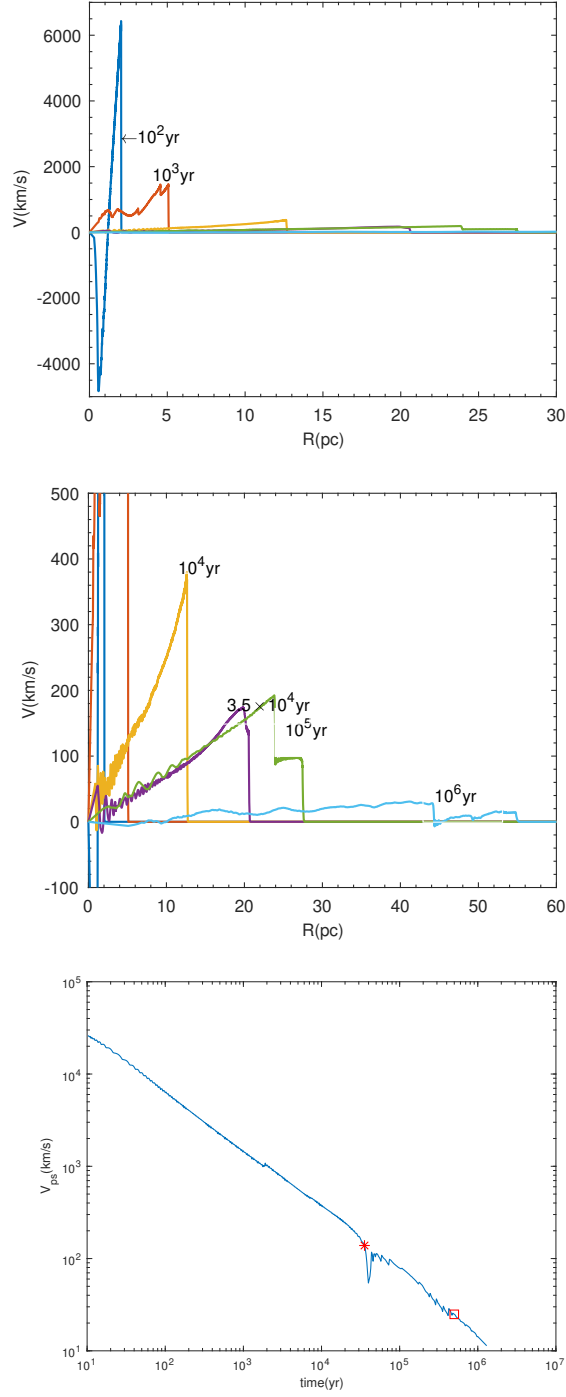


FIG. 1.— Subsequent velocity evolution of the GW170817 remnant. The top panel is the velocity profiles at 10^2 and 10^3 yr, the middle panel is the velocity profiles at 10^4 , 3.5×10^4 , 10^5 and 10^6 yr, the bottom panel is the velocity of the first shock vs time, in which star and square denote the time of the maximum luminosity and the end of cooling.

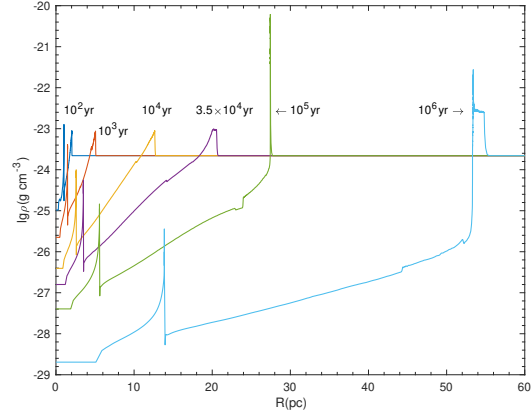


FIG. 2.— Density profiles of the GW170817 remnant at different time. The characteristic time are the same as that in Fig.1.

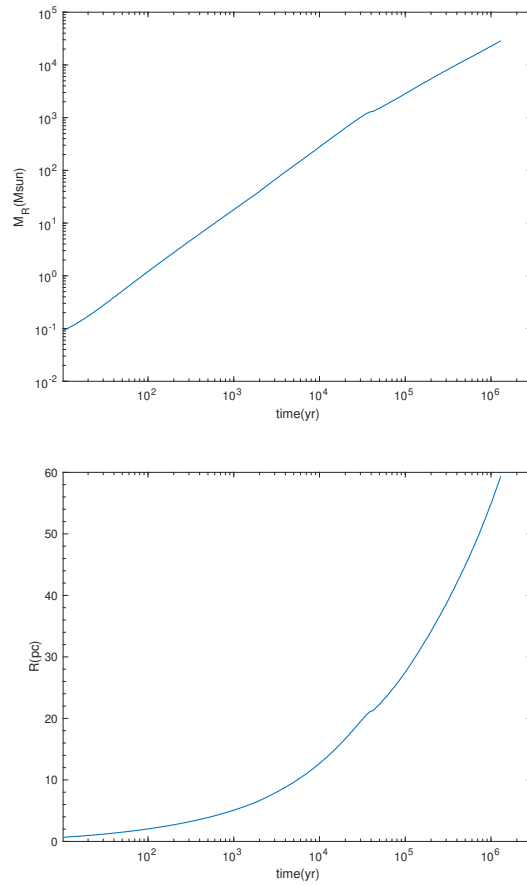


FIG. 3.— The mass (top) and radius (bottom) of the contaminated ISM as a function of time. The small circles and small squares represent the time when the luminosity is maximal and when the cooling ends, respectively.

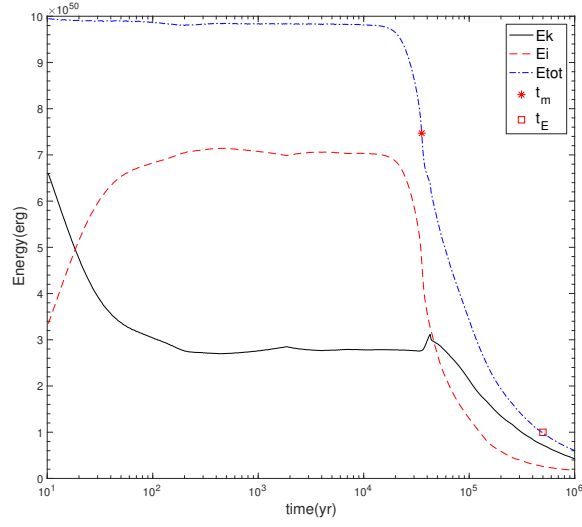


FIG. 4.— The energy of remnant as a function of time. The blue, red, and black lines are the total energy, internal energy and kinetic energy, respectively.

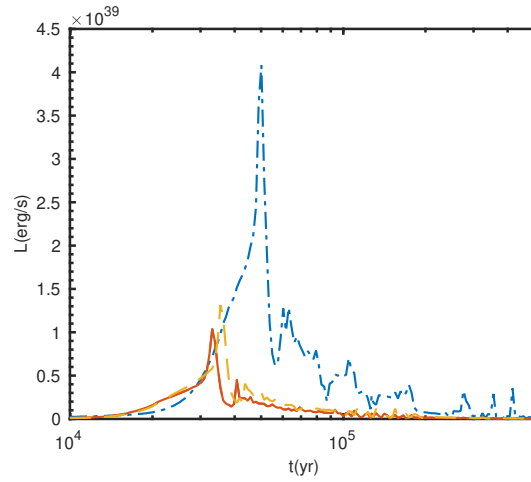


FIG. 5.— The luminosity of remnant as a function of time. The solid, dashed, and dot-dashed lines are luminosity corresponding to the ejecta mass of $0.001M_{\odot}$, $0.05M_{\odot}$, and $0.1M_{\odot}$, respectively.